HYPERVELOCITY IMPACT DAMAGE EQUATIONS FOR KAPTON MULTI-LAYERED INSULATION AND TEFLON SECOND-SURFACE MIRRORS

Michael J. Neish[(1)] and Seishiro Kibe[(2)]

[(1)]*Space Environment Measurement Group, National Space Development Agency, 2-1-1 Sengen, Tsukuba City, Ibaraki Prefecture 305-8505, Japan, E-mail: mike@nasda.go.jp*

[(2)]*Space Debris Research Group, Space Technology Research Center , National Aerospace Laboratory, 7-44-1 Jindaijihigashi-machi,Chofu City, Tokyo 182-8522, Japan, E-mail: kibe@nal.go.jp*

ABSTRACT

We report the results of recent hypervelocity impact tests into aluminised Kapton multi-layered insulation (MLI) and silverised Teflon second-surface mirrors (SSM), by means of an electrothermal gun. A comparison between the MLI and SSM impact perforations and those in pure Kapton and Teflon reveal large dimensional discrepancies.

An empirical equation is provided for MLI which, though restricted in its range of applicability, can be applied in the extraction of impactor characteristics from perforation hole diameters.

1. INTRODUCTION

The post-flight analysis of the Space Flyer Unit (SFU) [1, 2, 3] yielded flux information on about 800 impact craters in an area of approximately 15 m^2 of aluminised Kapton Multi-Layered Insulation (MLI) and FEP Teflon Second-Surface Mirrors (SSM). Some relationship between crater or perforation size and impactor velocity and diameter is required in order to extract impactor parameters from this substantial data set, and enable a comparison between this and other data from previous post-flight analyses. References [1], [2] and [3] provide structural details of SSM and MLI.

Impact feature measurements in MLI consist of simple perforation hole diameters, D_h – at the minimum point – in the top Kapton layer, which contained a thin deposited layer of aluminium on the back surface, thought to have a negligible effect on the cratering process. The relevant behaviour of the top MLI layer is therefore that of a single wall, for which a number of equations have been described for other materials.

In summary, Teflon SSM consists of a top FEP Teflon layer of thickness 127 µm, followed by thin silver and Inconel layers, adhesive (51 µm), and two aluminium sheets (381 µm each) sandwiching a honeycomb structure (1 cm).

The derivation of a damage equation for thermal control surfaces is hampered by the fact that MLI and SSM specifications differ from spacecraft to spacecraft. For instance, the LDEF thermal blankets consisted of a top layer of ~125-µm-thick FEP Teflon followed by another layer ~50-60 µm thick coated with silver and Inconel vapour deposits [4]. EuReCa MLI, on the other hand, consisted of an outer layer of beta-cloth about 200 µm thick, followed by one 75-µm layer of aluminised Kapton, followed by 19 layers of aluminised Kapton separated by thin Dacron nets and finally a 50-µm layer of aluminised Kapton painted on the rear side, for a combined thickness (excluding gaps) of about 600 µm [5, 6]. Hypervelocity impact calibration experiments are likely to focus on the specific thermal blanket design of interest to the investigator, and are probably not directly comparable to other thermal blanket designs, not to mention the properties of the pure material.

2. LIGHT-GAS GUN SHOTS AT 5 KM S^{-1}

The chosen strategy for the calibration shots is limited by the availability of samples. In our case the options were to fire at actual SFU spacecraft MLI (thickness of top layer = 50 µm) or at pure Kapton film. The latter is available to a maximum thickness of 175 µm, and so requires small projectiles if the interesting region between D_h/T = ~1-10 is to be investigated (where T is the film thickness). Since it is impractical (and expensive) to fire only one projectile of size ~100 µm each time, such shots are often handled using the buckshot technique whereby a number of projectiles are fired together using a sabot, providing a fairly large number of impact holes in one shot. This was also our chosen method, and proved very effective.

The first shots were carried out using the University of Kent (UKC) light-gas gun. The projectiles consisted of high-grade spherical soda-lime glass beads fired using the buckshot technique at 5 km s^{-1} at normal incidence. Strips of commercial Kapton film of various thicknesses were placed in a target holder so that one shot could provide data for several d_p/T ratios; four such shots were conducted.

The results, shown in Figure 1 are plotted in terms of projectile diameter versus hole diameter, both normalised to target thickness, and is the standard plotting format for thin-target perforations. For

comparison, the best-fit curves for pure FEP Teflon as obtained by Fred Hörz *et al*. in their excellent study of this material are also included [7, 8]. The horizontal error bars show the root-mean-square variation in hole diameter as measured for each sample of holes. Diameters were measured on the computer monitor by tracing out the margin of the inner wall of the impact hole and calculating the number of pixels within the area. This value was then converted to a circle enclosing the same area. The same approach was taken in the analysis of the SFU impacts; we chose it because it seemed capable of handling irregularities in the texture of the inner crater walls, conditions in which two diametric measurements taken at right angles might have given inaccurate values.

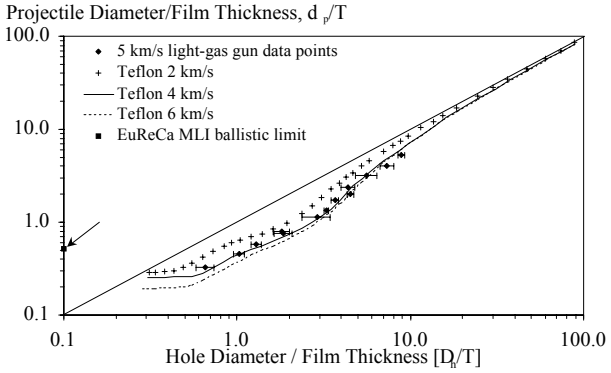

Fig. 1. Experimental data points derived from impact shots into Kapton film using a light-gas gun. Data points from a similar experiment into Teflon film [7, 8] are shown for comparison.

It is immediately obvious that the behaviour of Kapton mirrors that of Teflon very closely for a D_h/T range covering at least a factor of 20, albeit at a slightly different velocity. No data points currently exist to demonstrate whether this similarity extends all the way into the marginal perforation region on the left.

Also shown on the y-axis is a single data point at (0.1, 0.52), showing the ballistic limit of Kapton MLI from the EuReCa satellite for a projectile with the same composition and velocity as the ones used in the UKC tests. The ballistic limit of this arrangement conforms to the single-wall equation

$$F_{max} = 0.37 d_p^{1.056} \rho_p^{0.519} (V \cos\theta)^{0.875} \qquad (1)$$

derived from a series of tests carried out by J.C. Mandeville *et al.* [9], and so requires a projectile diameter of 312.5 μm, for a d_p/T ratio of 0.52 at the marginal perforation limit. Note that this value concerns complete perforation through the combined thickness of all the MLI sheets, ignoring the gaps in between, such that T = ~600 μm for EuReCa [10]. The discrepancy is due to the fact that the EuReCa MLI, being in fact a multi-walled target, behaves as a bumper shield, and therefore resists perforation more effectively. The data point is therefore intuitively well located with respect to the Kapton data.

The fitting equation chosen for the light-gas gun data is a variation of that derived by Gardner for metals [11]:

$$d'_p = A\left(\frac{10}{9+e^{\frac{D_h}{B}}}\right) + D'_h\left(1-e^{-\frac{D_h}{B}}\right) \qquad (2)$$

where $d'_p=d_p/T$, $D'_h=D_h/T$, e is the exponential constant, and A and B are various empirically-defined, material-related parameters. This equation has been modified in order to take into account the somewhat different shapes of the Kapton and Teflon curves as compared with metals. Thus, a two-parameter fit to the Kapton data has been obtained as follows:

$$\frac{d_p}{T} = 0.337 + \frac{D_h}{T}\left(1 - A^{\left(\frac{D_h}{T}+B\right)}\right) \qquad (3)$$

where the first term on the right-hand side of equation (2) is replaced by a constant, the exponential is replaced by a variable A (= 0.8912), which is raised to the power of D_h/T shifted by a variable B (= 0.06502). Two dummy data points were inserted to the left of the first data point, and another at the point (101,100) to ensure that the curve would exhibit the desired characteristics at the end points. In addition, various weightings had to be applied to all the points. The equation is, of course, not intended to be valid outside the range covered by the data points themselves, but assumes that the contour for Kapton will asymptotically approach $D_h = d_p$ as $D_h \rightarrow \infty$, and that the gradient will tend to 0 as $D_h \rightarrow 0$.

The change of gradient in the Kapton data around D_h/T = 1 to 2 in Figure 1 might be a real effect, rather than data point scatter, since FEP Teflon [7, 8] also displays similar characteristics around the same hole size range. However, a simple fit equation has been selected, pending confirmation by further experiments.

The Paul & Berthoud equations for D_{co} and D_{pit} in glass (cgs units) [12] are used to provide comparisons between pure Kapton and glass.

$$D_{co} = 5\times10^{-4} d_p^{1.076} \rho_p^{0.784} \rho_t^{-0.5} V_p^{0.727} \cos^{0.601}\Theta \qquad (4)$$

$$D_{pit} = 1.12\times10^{-4} d_p^{1.076} \rho_p^{0.743} \rho_t^{-0.5} V_p^{0.727} \cos^{0.15}\Theta \qquad (5)$$

D_{co} and D_{pit} versus D_h/T, for T = 25 μm, 50 μm and 100 μm are shown in Figures 2 and 3 respectively, valid for D_h/T > ~0.7.

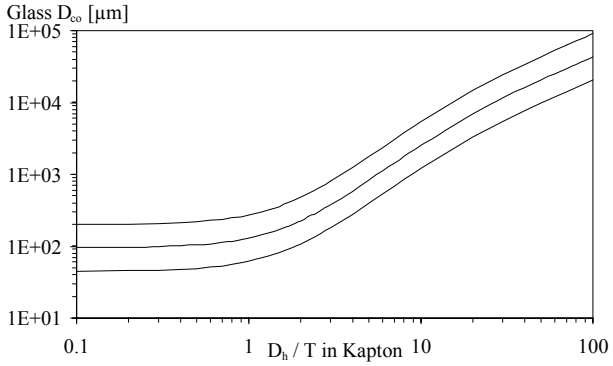

Fig. 2. Glass D_{co} versus Kapton D_h/T, at 5 km s^{-1}. From top to bottom: T = 100 μm, 50 μm and 25 μm.

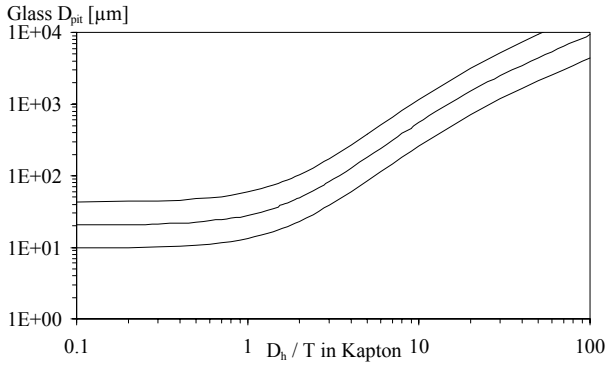

Fig. 3. Glass D_{pit} versus Kapton D_h/T, at 5 km s^{-1}. From top to bottom: T = 100 μm, 50 μm and 25 μm. Note the difference in the y-axis scale between Figures 2 and 3.

By inserting 2.3 g cm^3 for ρ_p, 2.16 g cm^3 for ρ_t, and 5 x 10^5 cm s^{-1} for V, the comparisons between D_{co} and D_{pit} in glass and Kapton film for the experimental parameters reduces to

$$D_{co} = 9.088(X \cdot T)^{1.076} \quad (6)$$

$$D_{pit} = 1.967(X \cdot T)^{1.076} \quad (7)$$

where X is the right-hand side of equation (3), and film thickness T is given in cm.

3. ELECTROTHERMAL GUN TESTS

A samples of SSM and MLI from the SFU spacecraft (hence exposed to space for ten months) were excised, and one shot into each was conducted using the electrothermal gun at Auburn University, extensively described in Reference [13]. Spherical soda-lime-glass grains of diameters – at impact, after ablation – ranging from around 20-200 μm were used. The gun is capable of attaining velocities of up to 15 km s^{-1}; the velocity range attained in these tests was 4-11 km s^{-1}, with a tendency for smaller projectiles to be faster.

Impact diagnostics were obtained by means of an X-Y detector and streak camera, which provided both position and velocity data. Projectile size was obtained from the hole left by each projectile in a thin layer of Mylar film (diameter 0.4 μm) placed at a stand-off distance of about 10 cm from the target. The projectiles were assumed to perforate this film with no loss of velocity or integrity. The results of the shots are summarised below.

3.1 SSM Target

3.1.1 Impact Morphology

The impact sites all possessed the same essential morphological features as those found in SSMs retrieved from space. However, there was more evidence of brittle failure and radial cracking reminiscent of glass, a feature almost entirely lacking in the space impacts, but which was observed by Hörz *et al*. [7, 8] in their light-gas gun tests.

The three main measurements taken of the sites, indicated in Figure 4, are the crater diameter D_c, which is the diameter of the inner Teflon wall of the central crater, D_r, the diameter of a ring lying outside the Teflon pit, on the same vertical level as the silver paint layer, and D_{delam} (also referred to as D_m), the delamination ring diameter, a line marking the outer limit of the area of detachment of the Teflon film from the underlying silver paint, usually several crater radii from the central hole. This latter feature is often not observed in smaller impacts.

In total, 15 sites of size D_c = 19-250 μm were obtained. The largest of these extended all the way into the aluminium honeycomb; the rest, (160 μm or less) were of the order of the Teflon film thickness, 127 μm, or smaller. Therefore thick target impact characteristics are expected, with some departure due to the presence of the underlying materials.

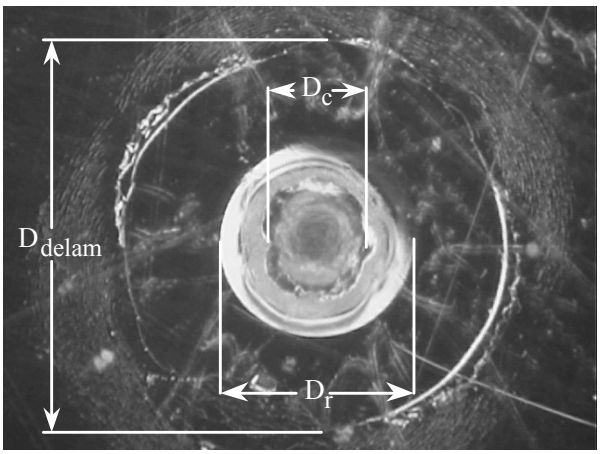

Fig. 4. Typical SSM impact feature.

3.1.2 Ratios

A plot of D_c/d_p as a function of impact velocity, V, is shown in Figure 5. Despite the invariable scatter, the data points appear to be well distributed. D_c/d_p increases with increasing V; a straight-line fit to the points (y = 0.039x + 0.97) approaches 1 with decreasing V.

However, a comparison between this data and the results of Hörz *et al*. for semi-infinite Teflon, shown in Figure 6, immediately reveals a large discrepancy between the two data sets. The Hörz *et al*. data possess a much higher gradient (0.44) indicating a greater sensitivity of D_c to V in semi-infinite Teflon. We have no reason to question the data, which were obtained from a thorough and well-controlled series of experiments. On the other hand, the data points from the SSM tests also appear to be internally consistent, thus reducing the probability of spurious results.

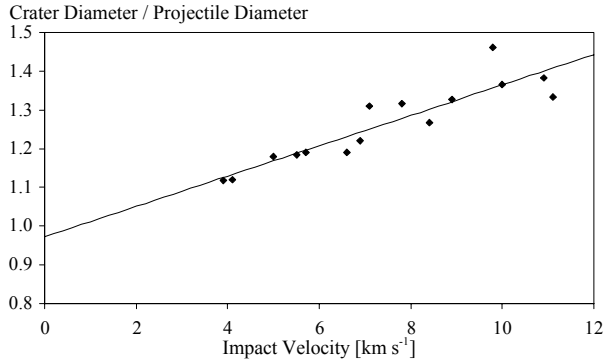

Fig. 5. Crater diameter normalised to projectile diameter versus impact velocity for the SSM impact tests.

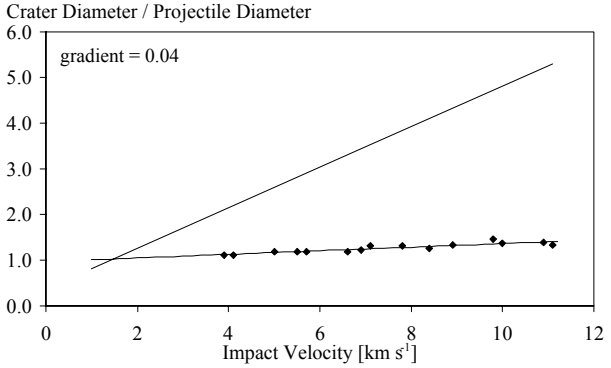

Fig. 6. A comparison of the SSM impact tests and previous tests on Teflon semi-infinite targets [7, 8].

It is noted, however, that both experimental conditions were not completely identical. Table 1 highlights three important differences.

With regard to the first point, one would expect slower D_c/d_p growth with respect to V to occur when the projectile size is large compared to the target thickness – i.e., when the thin target condition applies. This is certainly not the case in the SSM tests. The observed D_c/d_p ratio of 1-1.4 (strictly speaking D_h/d_p, when considering perforations) would be expected for hole sizes in excess of 10 times the target thickness, whereas the actual perforations are of the order of the film thickness or less. We therefore believe that this is not an adequate explanation, although the presence of the underlying materials must undoubtedly have an effect on the cratering process.

Table 1. Differences between the Teflon targets used in References [7] and [8] and the Teflon SSM target.

SSM Target	Teflon Target
complicated structure; thin top Teflon film with other materials underneath.	semi-infinite pure Teflon
exposed to the near-Earth space environment for ten months, then returned to Earth.	not exposed to space
projectile size range: 13-210 μm	projectile size: 3.162 mm

The second point in Table 1 implies that the hypervelocity impact characteristics of Teflon may have been altered by exposure to the space environment. It is known that the mechanical properties do change; the question whether hypervelocity impact properties are also affected naturally follows.

Thirdly, both experiments use very different projectile sizes; plotting them in terms of D_c/d_p in Figures 5 and 6 may hide any projectile size effects. However, the SSM tests span a projectile size range of over an order of magnitude; since the distribution of points in Figure 5 is unaffected, this does not appear to be the correct explanation.

There is the additional possibility that differences in the manufacturing processes of Kapton and Teflon for terrestrial or for space use could result in different hypervelocity impact properties.

Further tests into all these materials, pre-exposed and unexposed to the space environment, ought to resolve the issue.

Figure 7 is a plot of D_r/D_c versus V for SSM, showing no visible correlation between these parameters.

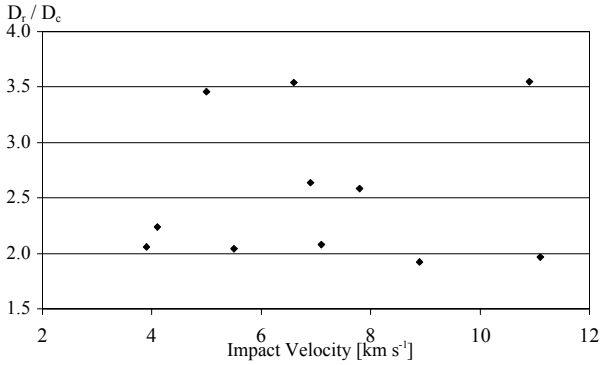

Fig. 7. D_r/D_c as a function of impact velocity.

3.2 MLI Target

Having obtained a d_p/T-D_h/T contour at 5 km s^{-1} for Kapton covering the size range of interest, the problem now becomes determining how this contour varies as a function of impact velocity.

The shot into MLI yielded 23 usable perforations at velocities ranging from 4.3 to 9.2 km s^{-1}. A plot of these points together with best-fit equation (3) is shown in Figure 8. The data points represent an assortment of d_p/T and D_h/T combinations at different impact velocities, and the task is to find a set of curves with the same general form as equation (3) which will best fit these points.

The data from both experiments are incompatible, however. The two points marked "+" are for an impact velocity of 5 km s^{-1}, and lie very far from the commercial Kapton curve for the same velocity. In fact, it is remarkable that many of the points lie very close to the y = x line, meaning that D_h is only slightly larger than d_p at velocities up to about 6.5 km s^{-1}. Indeed this observed effect is comparable to the fact that D_c/d_p in the SSM impacts was only slightly above 1, and a weak function of velocity.

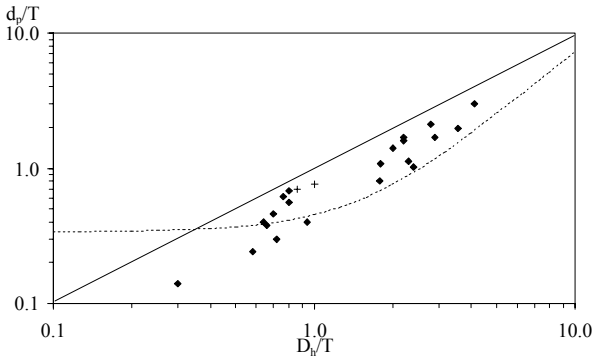

Fig. 8. Data points from the electrothermal gun shot into SFU MLI, with equation (2) for comparison.

Until a set of appropriate contours is derived with the help of more data, a series of straight lines in log-log space, though unrealistic, fits the data satisfactorily, within the size and velocity limits of the experiment. Since this also corresponds with the typical micrometeoroid and space debris impact holes observed in retrieved MLI surfaces, they can be applied to the determination of impactor diameter from hole size, if an average normal impact velocity is assumed. The equation is as follows:

$$\frac{d_p}{T} = A \frac{D_h}{T} V^B \qquad (8)$$

[valid range: V = 4 – 9 km s^{-1}; D_h/T = 0.5 – 4]

where A = 4.09371 and B = -1.0671. The unweighted least-mean-square value is 0.082, and the mean error magnitude for all the points is only 7.92%. The contours are shown below in Figure 9.

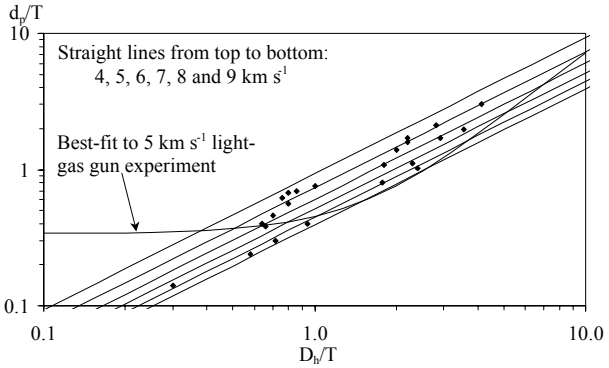

Fig. 9. Straight-line velocity contours in log-log space fitted through the MLI electrothermal gun data.

4. CONCLUSIONS

There is a large discrepancy in impact feature diameters between tests carried out into SSM and MLI that have been exposed to space, and into pure Teflon and Kapton. The reason for this is not clear: of the four possible explanations that we offer, the most plausible may be that differences in the manufacturing processes result in different hypervelocity impact properties. Calibrating the pure, commercial materials for application to spacecraft thermal control surfaces therefore seems inappropriate, but more precise tests aimed at elucidating the differences are required to verify this.

Post-flight analysis data of the SFU spacecraft also support the observation made in the impact calibration shots that the impact site dimensions in SSM and MLI are comparable. Figure 10 shows the SSM and MLI fluxes for Payload Units 1 and 4 which pointed +24° and -24° respectively from the spacecraft ram direction, and were negligibly shielded by the solar arrays; the fluxes from both surfaces have been combined together to improve the statistics.

The left-hand sides of both curves in Figure 10 (below about 70 μm) show the typical roll-off that occurs for scanned surfaces. In addition there are too few impacts in the right-hand region, for large hole sizes, to allow a reliable comparison between both materials. The workable region is therefore around ~70 to 200 μm, within which both flux curves lie close together, with the MLI hole size slightly larger than the SSM D_c for the same flux. A crossing-over occurs around 170 μm after which D_c in Teflon steadily diverges from MLI D_h. This is due to a morphological change that occurs in the SSM impact craters around this size [3], above which the entire top Teflon film is detached from the underlying silver paint, up to a certain distance away

from the impact centre, and raised upwards. Crater formation in this region is therefore governed by different physical processes.

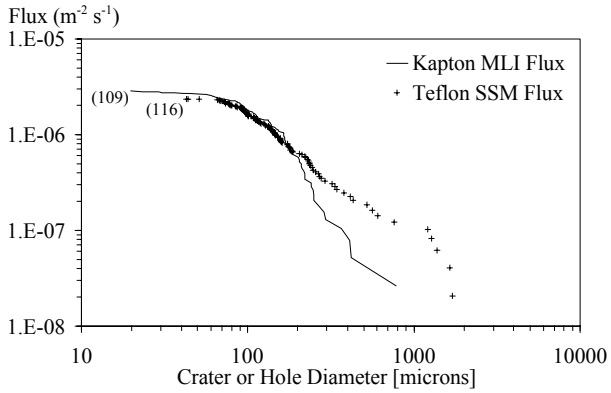

Fig. 10. PLU-1 and 4 MLI and SSM fluxes combined together. The number of impacts on each surface is shown in the brackets.

We will attempt more hypervelocity impact tests to improve the empirical equations for both MLI and SSM, with post-flight-analysis data assisting in making material cross-comparisons. In view of the ubiquity of thermal control surfaces on satellites, and the possibility of more post-flight analyses always present, we believe that more accurate damage equations for these materials ought to be derived.

5. REFERENCES

1. M. J. Neish, H. Yano, S. Kibe (2000). "Data Analysis Micrometeoroid and Debris Fluxes as Measured on the Space Flyer Unit", *Proc. International Space Tech. And Science Symposium,* Morioka, Japan, May 2000.
2. M. J. Neish, S. Kibe, H. Yano, S. P. Deshpande, K. Morishige (1999). "Post-Flight Analysis of the SFU: Current Status and Future Plan", *Adv. Space Res., Vol. 23, No. 1*, pp. 101-111.
3. M. J. Neish, S. P. Deshpande, S. Kibe, H. Yano, Y. Kitazawa, S. Yamamoto (1997). "Micrometeoroid and Space Debris Impacts on the Space Flyer Unit, and Hypervelocity Impact Calibration of its Surfaces", *Second European Conference on Space Debris, ESOC, Darmstadt, Germany, 17-19 March 1997, ESA Publication SP-393*, pp. 177-182.
4. D. O'Sullivan, A. Thompson, J. Bosch, R. Keegan, K. P. Wenzel, A. Smit and C. Domingo (1992). "The LDEF Ultra-Heavy Cosmic Ray Experiment", *in LDEF-69 Months in Space, First Post-Retrieval Symposium, NASA Conference Publication CP-3134*, pp. 367-376.
5. G. Drolshagen (2000). "Shielding Effectiveness of MLI", *ESA Document EMA/00-018/GD*.
6. G. Drolshagen (1995). *ESA Internal Note* WMA/95-076/GC/MLI.
7. F. Hörz, M. J. Cintala, R. P. Bernhard, T. H. See, T. (1995). "Cratering and Penetration Experiments in Teflon Targets at Velocities from 1 to 7 km/s", *Int. J. Impact Engng.*, Vol. 17, pp. 419-430, Elsevier Science Ltd, 0734-743X/95.
8. F. Hörz, M. J. Cintala, R. P. Bernhard, F. Cardenas, W. Davidson, G. Haynes, T. H. See, J. Winkler, J. Knight (1994). Cratering and Penetration Experiments in Teflon Targets at Velocities from 1 to 7 km/s, *NASA Technical Memorandum, TM-104797*.
9. J. C. Mandeville *et al*. (1998). *Final Report of ESA Contract 11540/95/NL/JG, ESA CR (P) 4214*.
10. G. Drolshagen (2000). *Private communication*.
11. D. J. Gardner (1995). "Hypervelocity Impact Morphology", *Ph.D. Thesis*, University of Kent at Canterbury, Kent, U.K.
12. K. G. Paul & L. Berthoud (1995). "Empirical Scaling Laws for Crater Dimensions for Impacts into Solar Cells", *Proc. IAU Colloq. No. 150*, "Physics, Chemistry and Dynamics of Interplanetary Dust", Gainesville, Florida.
13. S. R. Best, and M. F. Rose (1999). "A Plasma Drag Hypervelocity Particle Accelerator (HYPER)", *Int. J. Impact Engng., Vol. 23*, pp. 67-76.